photonics

MDPI

Article

A Hybrid Simulated Annealing Approach for Loaded Phase Optimization in Digital Lasers for Structured Light Generation

Ying-Jung Chen, Kuo-Chih Chang, Tzu-Le Yang and Shu-Chun Chu *

Department of Physics, National Cheng Kung University, No. 1, University Road, Tainan City 701, Taiwan; l26104181@gs.ncku.edu.tw (Y.-J.C.); kcchang@gs.ncku.edu.tw (K.-C.C.); c24096017@gs.ncku.edu.tw (T.-L.Y.)
* Correspondence: scchu@mail.ncku.edu.tw

Abstract

This study proposes a method for designing spatial light modulator (SLM) projection phases in digital lasers using a simulated annealing (SA) approach combined with an initialized pre-designed phase to generate structured laser beams. SLM projection phases are optimized within the SA framework using a cost function based on the correlation between the corresponding laser field patterns and the target field. Numerical simulations demonstrate both the effectiveness of the proposed phase design method and its improvement in generating three geometric beams—quadrangular pyramid, triangular pyramid, and multi-ring fields—particularly with regard to enhanced edge sharpness. The resulting structured beams, especially those with simple geometric shapes, are suitable for microfabrication applications such as photolithography and photopolymerization. The proposed SA iteration framework is not limited to the L-shaped resonator used in this study and can be extended to digital laser cavities with higher numerical apertures, enabling the generation of more complex structured light fields.

Keywords: digital lasers; simulated annealing; spatial light modulator; beam shaping; structured light fields

Received: 8 September 2025
Revised: 1 October 2025
Accepted: 9 October 2025
Published: 13 October 2025

Citation: Chen, Y.-J.; Chang, K.-C.; Yang, T.-L.; Chu, S.-C. A Hybrid Simulated Annealing Approach for Loaded Phase Optimization in Digital Lasers for Structured Light Generation. *Photonics* **2025**, *12*, 1005. https://doi.org/10.3390/photonics12101005

1. Introduction

The well-developed beam shaping techniques [1–13] enrich the applications of structured laser beams [14–32]. The outer cavity beam shaping method converts the laser output into an on-demand light field through extra-cavity optical design [2,3]; in contrast, the intra-cavity beam shaping relies on the cavity design, where the on-demand light field is directly generated within the laser system [4–7]. The recently developed digital laser introduces a dynamically adjustable optical element, a pure phase-control spatial light modulator (SLM), as part of the cavity boundary, effectively expanding the possibilities and flexibility of intra-cavity beam shaping [8–13]. Digital laser was first proposed by Ngcobo et al. in 2013 [9], and several typical laser beams with analytical forms, such as Hermite-Gaussian beams, Laguerre-Gaussian beams, Airy beams, etc., were successfully generated. Next, the polarization control [33] and second harmonic generation [34] of high-order laser modes in digital lasers were achieved. In addition, the development of digital lasers also turned to the discussion of generating light fields with on-demand structures [8–13] because the real-time manipulation of the laser output profile, such as via photolithography [14–16] and photopolymerization for microfabrication, is expected to be beneficial to structured beam applications [21–25,35]. Several methods have been proposed for generating laser beam with specific geometric shapes in digital lasers, such as circular flat-top beams [8], doughnut

beams [13], and uniform/flat beams with arbitrary lateral distribution [10–12]. Tradonsky et al. proposed a method to generate complex-structured beams of low-spatial-coherence from digital lasers using a degenerate cavity, intracavity spatial filtering techniques, and experimental feedback algorithms [36]. However, the method is restricted to degenerate cavities, and the super-pixel approach it employs reduces effective SLM resolution. Most importantly, the optical field iteration inherent to this method substantially increases the complexity and size of the optical system. Recently, Chu et al. proposed a convolution method in designing the SLM projection phase diagram for generating light intensity of a specified geometric shape [12]. In the method, the phase boundary of the digital laser was designed to match the convolution of the specified geometric structure with a Gaussian field, rather than the geometric structure directly. That is, the convolution method generated a weighted multi-point Gaussian field that serves as a good approximation of the specified structured laser field. Although the laser field generated by the convolution method closely resembles the on-demand light field, deviations are inevitable, especially in sharp regions such as the apex or edges of a cone-shaped field.

The simulated annealing (SA) algorithm, first proposed by S. Kirkpatrick et al. in 1983 [37], is a heuristic optimization algorithm inspired by annealing process of solids. It is a well-known and effective approach for global optimization. By defining an appropriate cost function, the SA method can optimize the system performance according to specific requirements. The SA method has also been applied to deal with various practical issues [38–40], including outer-cavity beam shaping [41–43]. For example, R. El-Agmy et al. developed a method to generate on-demand Gaussian and super-Gaussian beams that adaptively match the desired target profile using a deformable mirror [41]. Recently, Hu et al. used the SA method in the optimization of brightness in an Nd:YAG laser by maximizing the single-mode power factor with an intra-cavity SLM [44]. However, this method is limited to power optimization for specific eigenmodes of the laser resonator and cannot be used to find light fields with arbitrary structures. The intra-cavity element of digital lasers, a pure phase-control SLM, as a pixelated step-level-phase optical element, is well suited for SLM phase design using numerical optimization techniques. In this study, we propose an optimization approach for designing the SLM projection phases of digital lasers to generate laser intensity distributions of specified shapes, using the SA method combined with an initialized pre-designed phase from the convolution method. Three types of laser fields are demonstrated: quadrangular pyramid, triangular pyramid, and multi-ring fields. The results indicate that the laser field distribution can be optimized by adjusting the SLM projection phases using the proposed approach. With this SLM phase design method, laser patterns superior to those obtained with the previous convolution method [12] were achieved. The optimization approach presented in this study is not limited to the L-shaped digital laser employed here and can be extended to other digital laser cavities with higher numerical apertures, enabling the generation of structured light fields with greater complexity.

2. Simulation Method

Section 2.1 describes the simulation framework adopted in this study for digital laser output, i.e., laser configuration, parameters, and the methods for simulating a laser oscillation beam. Section 2.2 explains the approaches to implementing the SA algorithm to optimize the phase boundary of the laser cavity. All simulations were conducted using in-house developed codes implemented in MATLAB (MathWorks, Natick, MA, USA, version R2022b).

2.1. Laser Configuration in Simulation

Figure 1a shows the configuration of the digital laser system used in this study, a diode-pumped solid-state laser (DPSSL) using a common L-shape laser cavity in several digital laser studies [9,11,12]. The cavity consists of an SLM panel, a partially reflective mirror (PM), and the laser crystal. The 45°-tilted PM serves as the output coupler of the laser system. The coated crystal surface and the reflective panel of the SLM constitute a typical two-mirror optical cavity. Figure 1b shows the equivalent light path diagram of the laser system.

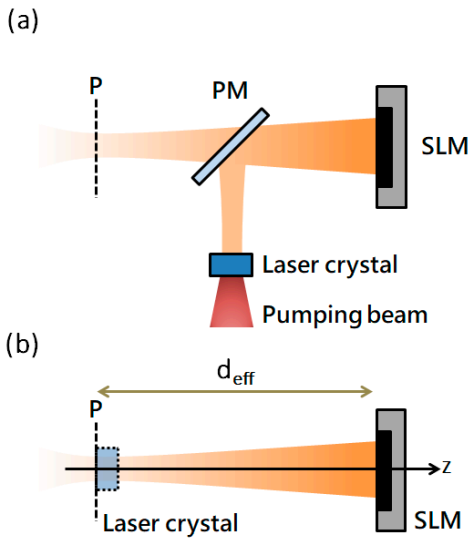

Figure 1. Laser configuration used in simulations. (**a**) a typical L-shape digital laser, plane P is the observation plane of the output beam. (**b**) An un-folded equivalent two-mirror laser cavity of an L-shape laser cavity.

This study employed the method proposed by Endo [45–47] to simulate the intracavity oscillating field, i.e., the convergent lasing field of the laser system. The method has been applied in searching for single- or multi-mode convergent oscillation light field in both stable and unstable DPSSL cavities [48–50]. In this method, the initial spontaneous emission with random phases and directions was propagated and diffracted within the laser cavity, experiencing homogeneously broadened gain during each pass through the crystal. Ultimately, the intra-cavity oscillating light field converged to the lasing pattern of the cavity. The simulation parameters used in this study are detailed as follows. The laser crystal is a 1 mm thick Nd:YVO_4 crystal with 100%-reflectance on one side at the lasing wavelength of 1064 nm. The reflectance of PM at 1064 nm is 97%. The SLM panels provide 1024-step digital phase modulation over a 2π range, with a pixel size of 8.0 μm. The phase diagram loaded onto the SLM was generated by digitalizing the full phase cycle of 0 to 2π into 1024 levels. Referring to a laser configuration mentioned previously [12], the effective cavity length of the two-mirror cavity, d_{eff}, was set as 25.6 cm. In this study, the output field was optimized for observing plane P (see Figure 1), corresponding to the coated reflective surface of the crystal in the cavity.

2.2. SA Method in Designing Spatial Light Modulator Projected Phase Diagram

This study employed the SA method to determine the SLM projected phase diagram ϕ of a digital laser for optimized laser output. Figure 2 shows the flow chart of the SA algorithm of this study. The SA method imitates the slow cooling process of metal to search for the global optimum. Next, we define each parameter used in the flow chart and then explain the iterative process.

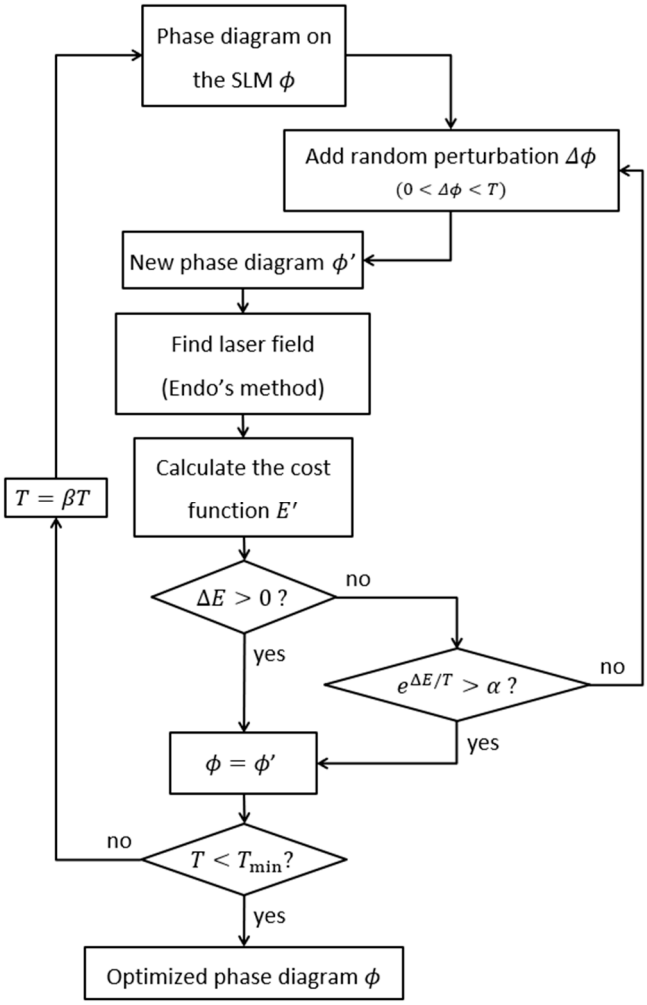

Figure 2. Flow chart of the simulated annealing algorithm for optimizing the phase diagram on the spatial light modulator (SLM).

In this study, the quality of the output laser field was evaluated by a cost function E, defined as

$$E = C_{\text{corr}}/k, \tag{1}$$

$$C_{\text{corr}}(A, B) = \frac{1}{M \times N - 1} \sum_{m=1}^{M} \sum_{n=1}^{N} \left(\frac{A_{mn} - \mu_A}{\sigma_A} \right) \left(\frac{B_{mn} - \mu_B}{\sigma_B} \right) \tag{2}$$

where k is a constant, as explained later. C_{corr} is the correlation coefficient between the specified target field, represented by matrix A, and simulated lasing field, represented by matrix B. Here, A_{mn} and B_{mn} denote the elements of matrices A and B; μ_A and μ_B are the means of matrices A and B; σ_A and σ_B are the standard deviations of matrices A and B; and M and N are the number of data points along the x and y axes of matrices A and B, respectively. The SA method involves three key parameters governing its convergence: T, β, and T_{min}. T denotes the system "temperature." After each iteration, T decreases to βT, where β is the cooling factor ($0 < \beta < 1$) that directly controls the cooling rate. The iteration continues until T reaches T_{min}, the lower limit of temperature. α is a computer-generated random number within (0, 1), which dynamically influences whether to accept the current solution as the initial solution for the next iteration.

The iterative process is described as follows. As shown in Figure 2, the iteration starts from an initial (random or specified) phase diagram, ϕ. In this study, T controls the phase perturbation scale in each iteration loop. At the beginning of every iteration, a random perturbation was added to the initial phase diagram within the range (0, T) resulting in a

perturbed phase diagram $\phi\prime$. Then, the new phase diagram $\phi\prime$ was applied to the digital laser. The resulting laser field was numerically obtained using Endo's method [45]. After that, the laser quality was calculated by the cost function E, and the difference ΔE was then computed as $\Delta E = E' - E$, representing the change in the cost function between the perturbed and unperturbed phase diagrams. When $\Delta E > 0$, it indicates that the laser field is closer to the target field; in other words, the perturbed phase diagram $\phi\prime$ represents a better solution than the unperturbed phase diagram ϕ. In this case, $\phi\prime$ was accepted as the starting phase diagram ϕ in the next iteration. Otherwise, under the conditions proposed by Metropolis et al. [51], acceptance was tested using $\exp(\Delta E/T) > \alpha$. The inferior solution ($\phi\prime$) has a chance of being accepted as the next starting phase (ϕ).

Here, α is a general random number within (0, 1), and thus, this study introduced a constant k in the cost function to adjust the acceptance probability of an inferior solution ($\phi\prime$) as the new solution for starting the iteration. The value of k affects the magnitude of $\exp(\Delta E/T)$, allowing the probability of accepting an inferior solution to be adjusted for different correlation values. For example, with the value k = 0.0003 used in this study and an initial temperature of T = 0.1, when the correlation difference is on the order of 10^{-4}, $\exp(\Delta E/T)$ is approximately 3%, whereas when the correlation difference is on the order of 10^{-5}, $\exp(\Delta E/T)$ is around 70%. Note that the probability of accepting an inferior solution allows the SA method to escape local optima and potentially reach the global optimum. If the inferior solution is not accepted, a new perturbed phase diagram $\phi\prime$ is generated. After each update of the phase diagram ϕ, the temperature T is reduced by the cooling factor β, and the iteration is repeated. As the temperature gradually decreases, the perturbation applied in subsequent iterations also decreases. Finally, the iteration terminates when T reaches $T_{\min}$.

2.3. Phase Initialization

In the conventional SA method, the initial phase usually starts from random, which may lead to slow convergence or trapped in the suboptimal local minimum. Moreover, achieving satisfactory results may require many iterations, which are computationally expensive. The previous convolution method [12] leverages the inherent stability of fundamental Gaussian beams inside the cavity and utilizes a Gaussian-convolved target field to construct a SLM projection phase that leads to the stable lasering of the desired target geometric laser field. However, a known limitation of the convolution method is that it tends to smooth sharp features, resulting in blurred edges and softened corners in the generated laser intensity distribution, as it is inherently tied to the Gaussian-convolved target design.

In this study, we propose a hybrid strategy: using the phase distribution generated by the previous convolution method as the initial phase solution for the SA algorithm. By starting from a more structured and physically meaningful initial phase, the hybrid strategy is expected to converge faster and produce higher quality fields within a limited computational budget.

2.4. Target Field

This study used three kinds of light fields as the target generating field of digital lasers to verify the proposed method of digital laser light fields optimization. Three target laser fields were the quadrangular pyramid, triangular pyramid, and multi-ring light field. The quadrangular pyramid field is defined as a linear intensity distribution decreasing symmetrically from the center, given by:

$$I(x, y) = \max(0, h - a \times \max(|x|, |y|)) \quad (3)$$

where the max function returns the maximum value among its input arguments, $h = 1$ is the peak intensity, and $a = 2 \times h/w$ is the slope, $w = 600$ μm is the base width, which defines the field's support region as $-w/2 \leq x, y \leq w/2$, values outside this region are set to zero.

The triangular pyramid target field is generated based on a tetrahedral geometry. The base of the pyramid is an equilateral triangle of side length $w = 600$ μm, and the apex is located vertically above the triangle at height $h = 1$. The intensity profile is computed as the minimum of three planar functions representing the pyramid facets:

$$I(x, y) = \max(0, \min(p_1(x, y), p_2(x, y), p_3(x, y))) \tag{4}$$

where the min function returns the minimum value among its input arguments, each $p_i(x, y)$ corresponds to the plane equation of the triangle facets. Values outside the pyramid region are set to zero.

The multi-ring target field consists of four identical annular intensity distributions centered at position $(x_i, y_i) = (\pm a_3/2, \pm a_3/2)$. Each ring has an inner radius $a_1 = 175$ μm, outer radius $a_2 = 225$ μm, and the intensity in each ring is set to 1 and 0 elsewhere. Mathematically, the field is constructed as:

$$I(x,\ y)\ =\ \sum_{i=1}^{4} \begin{cases} 1, & a_1 \leq \sqrt{(x - x_i)^2 + (y - y_i)^2} \leq a_2 \\ 0, & \text{otherwise} \end{cases} \tag{5}$$

3. Simulation Results and Discussion

For comparison with the convolution method [12], the proposed SA method was employed to determine the optimal SLM projection phases for generating three geometric light fields in a digital laser—quadrangular pyramid, triangular pyramid, and multi-ring fields—as in the referenced work. In this section, all the simulation results are normalized to peak intensity for ease of comparison. The SA algorithm was implemented with same parameters as the initial temperature $T = 0.1$, $\beta = 0.9997$, $T_{\min} = 0.01$, $k = 0.0003$, total iterations of 7675.

First, we perform a comparative analysis of quadrangular pyramid fields generated in a digital laser using SLM phases designed by three methods: (1) the convolution method, (2) the SA method with a random initial phase, and (3) the SA method initialized with the convolution-derived phase. The improvement of the SA method over the convolution method is demonstrated by comparing the correlation and the peak-to-valley error between the obtained laser field and the target field. The correlation involves direct calculation through the basic definition [52,53], and the peak-to-valley error is calculated from the difference between the normalized generated field and the curve-fitting field. The results are shown in Figure 3. The top row (a–c) displays the 2D intensity profiles of the resulting fields. Among these, the field generated by the SA method initialized with a convolution-derived phase (c) shows the highest correlation with the target pattern (correlation = 0.997), whereas the randomly initialized SA result (b) exhibits a lower correlation (correlation = 0.900) and noticeable scattered light in the outer regions of the field (see Figure 3k). The second row (d–f) shows the 3D view of the field intensity, where the convolution results (d) demonstrate smoother profiles than those in (e) and (f). The third row (g–i) compares the cross-sectional intensity distributions along the y-axis against the curve-fitting target quadrangular pyramid field. The results from the convolution method (g) and convolution-initialized SA (i) closely match the ideal curve, while the randomly initialized SA method (h) deviates more significantly. Finally, the bottom row (j–l) presents intensity difference maps between the generated field and the curve-fitting target fields. The peak-to-valley errors are 0.2268 for (j), 0.4706 for (k), and 0.1740 for (l), indicating that the proposed hybrid phase design strategy yields a laser field with the least residual error relative to the target field.

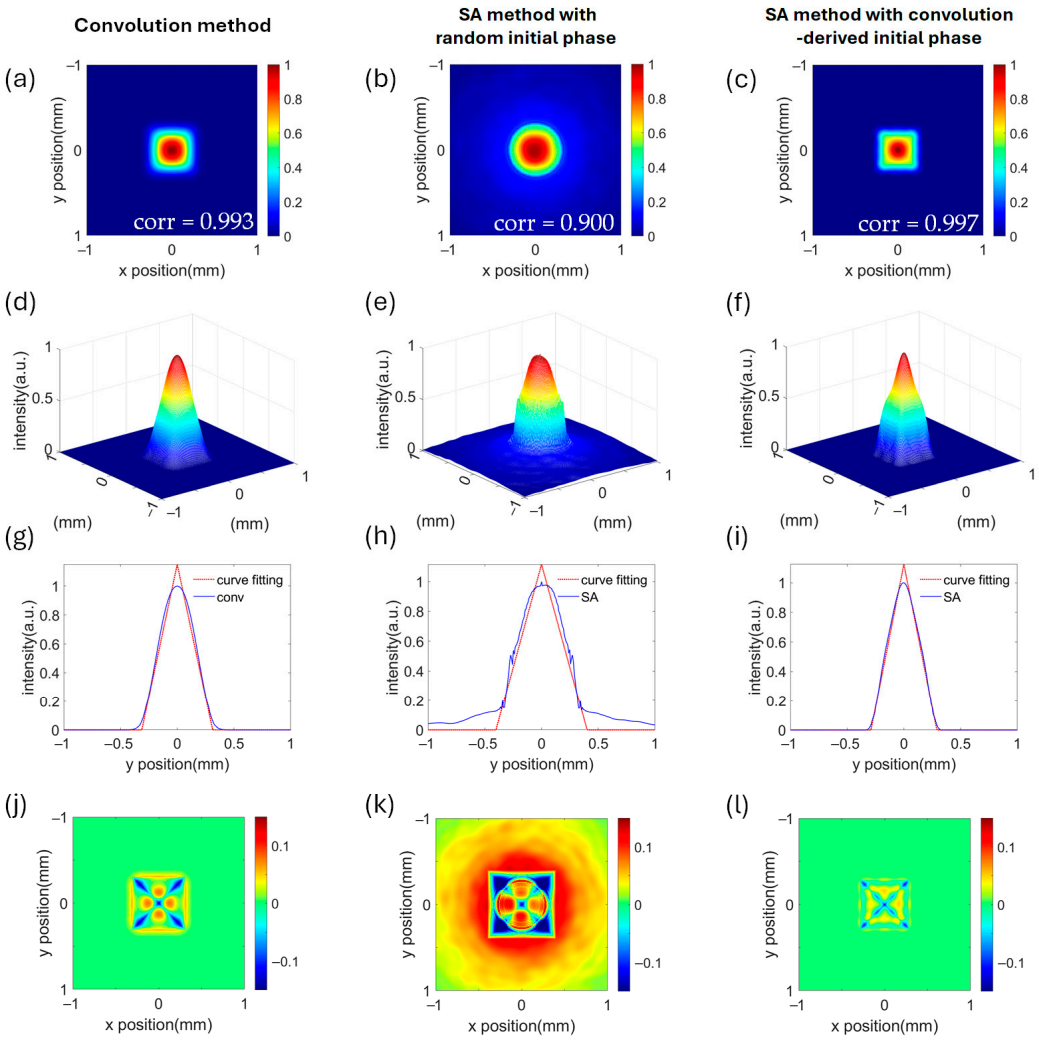

Figure 3. Comparison of quadrangular pyramid field intensity distributions obtained using three SLM phase design methods: the convolution method (**left column**), the SA method initialized with a random phase (**middle column**), and the SA method initialized with the convolution-derived phase (**right column**). Panels (**a**–**c**) show the planar views of the intensity profiles, (**d**–**f**) show the corresponding 3D views, (**g**–**i**) show the cross-sectional intensity distributions along the *y*-axis compared with the closest target fields (curve-fitted target fields), and (**j**–**l**) show the intensity differences between the obtained laser fields and their corresponding target fields.

In fact, the previous convolution method aims to generate a Gaussian-convoluted field that approximates the target field; as a result, it exhibits smoothed edges. As revealed by the results in Figure 3d, the four edges extending from the center to the base corners appear less sharp, resulting in softened transitions rather than well-defined ridgelines. The pyramid apex is rounded, lacking the sharp characteristics of the target field. Along the base plane, the intensity variation is relatively gradual, failing to reproduce the steep gradients of the target. Consequently, the outer boundaries of the structure appear blurred, and the lower corners of the pyramid lack clear definition. These observations indicate that, while the convolution method captures the general geometry of the target, it tends to smooth out finer structural details due to the intrinsic averaging effect of Gaussian convolution. The results in the middle column of Figure 3 show that, when the SA method is initialized with a random phase, it is difficult to find solutions that outperform the convolution method using a non-sufficiently gradual annealing procedure. A slower annealing process, however, would require a greater number of iterations and increased computation time. In contrast, the field obtained from the SA method initialized with the convolution-derived

phase (right column, Figure 3f) exhibits significantly sharper structural features that more closely match the target field. The pyramid apex becomes noticeably pointed, resembling a spike rather than the dome observed with the convolution method. Along the base, the intensity transitions are steeper and more abrupt, providing a closer match to the sharp edges of the target. Moreover, the four edges connecting the apex to the base appear much sharper, indicating improved preservation of high spatial frequency components. These improvements demonstrate that initializing the SA method with the convolution-derived phase enhances its convergence, allowing the algorithm to reach the desired structure more efficiently. At the same time, this approach avoids the smoothing effect inherent in the convolution method and preserves both the overall geometry of the target field and its fine structural details.

To further validate the generality of this approach, Figure 4 presents the results for two other target fields—a triangular pyramid field and a multi-ring field—as comparative examples. The figure shows the intensity distributions of the triangular pyramid (top row) and the multi-ring field (bottom row) generated using the convolution method and the SA method initialized with the convolution-derived phase.

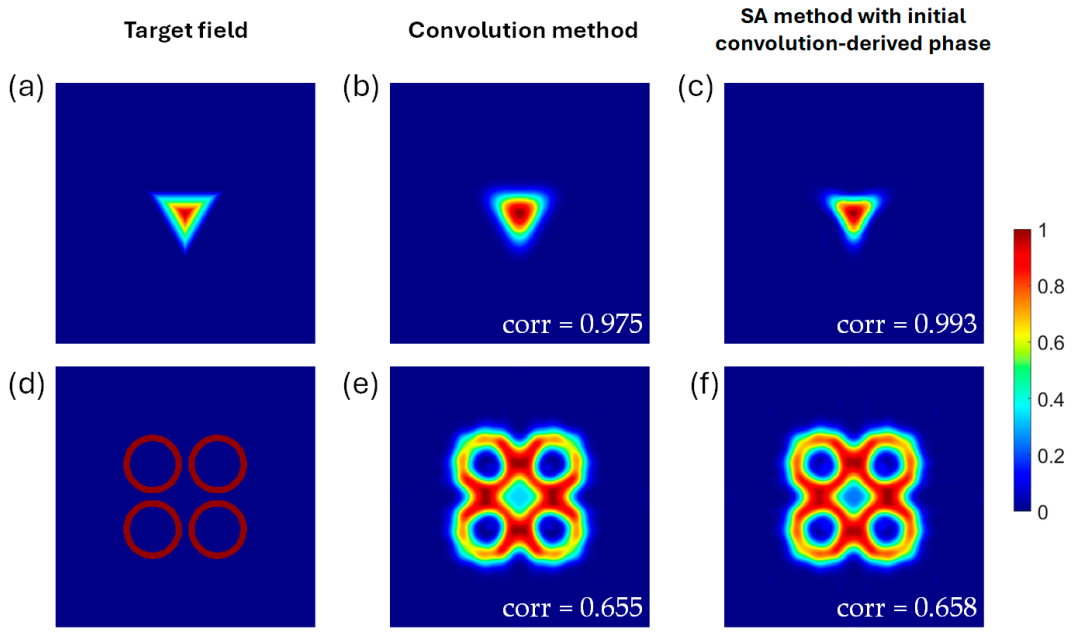

Figure 4. Intensity distribution of the target field (**left column**), the field obtained from the convolution method (**middle column**), and the SA method initialized with the convolution-derived phase (**right column**). (**a**–**c**) present the intensity profile of the triangular pyramid field. (**d**–**f**) present the intensity profile of the multi-ring field.

For the triangular pyramid field (Figure 4a–c), the field generated by the convolution method can capture the general triangular shape of the target, but the edges and apex are smoothed. The transitions between the faces are rounded, and the corners are less sharp than those of the target field. The SA method with initial phase of the convolution method yields the field with sharper apex and edges, thus more closely matching the target field. Similarly, for the multi-ring field (Figure 4d–f), both methods reproduce the overall multi-ring structure; however, despite the SA method yielding slightly higher correlation values than the convolution method, both results still show clear deviations from the target field. The intensity distribution between the rings departs from the desired profile, particularly in terms of contrast sharpness and boundary definition, and the correlation values remain relatively low. These deviations may result from the limited angular spec-

trum coverage of the current L-shaped resonator configuration, which is insufficient to support the reconstruction of highly complex structured light fields. The close spacing between rings imposes higher requirements on the spatial resolution of the intra-cavity field, whereas increasing the ring spacing can lead to improved results. However, this highlights the necessity of using laser cavities capable of supporting a broader angular spectrum range, such as degenerate cavities [36], to generate more complex structured light fields. On the whole, the results in Figures 3 and 4 demonstrate that the proposed SA-based hybrid strategy consistently outperforms the convolution method in generating structured light fields.

Overall, when the SLM phase was designed using the proposed SA method initialized with the convolution-derived phase, the digital laser produced a field pattern that more closely matched the specified target than that obtained with the previous convolution method, particularly exhibiting enhanced tip and edge sharpness. The present study aims to investigate, through numerical simulations, whether the design of SLM projection phases can be improved using only the measured laser field in combination with SA-based optimization, so that the laser output more closely matches the target field. Importantly, the proposed SA method for SLM phase design is not limited to the L-shaped resonant cavity digital laser used in this study. Employing a digital laser cavity with a higher numerical aperture [36] is expected to enable the generation of structured beams with greater complexity. Furthermore, with reference to the SA iteration flowchart (Figure 2), the "Find laser field" step in this numerical study involved obtaining the laser output by simulating an ideal system with homogeneous gain. The proposed iterative method could also be applied to various digital laser systems if this step is replaced by direct measurement of the laser output. When applied to a real digital laser, all controllable and uncontrollable system errors—such as crystal and lens thermal effects, element alignment errors, and manufacturing imperfections—would be inherently incorporated into the system as linear or nonlinear phenomena, allowing the optimization to achieve adaptive beam profile control. These potential extensions of the current study merit further exploration in future work.

The performance of a digital laser is inherently constrained by the specifications of the SLM, such as its thermal threshold, diffraction efficiency, and resolution, which together determine the achievable output power, spatial resolution, and lasing threshold. For example, with regard to the SLM damage threshold, the adopted Santec SLM-300 has a thermal damage threshold of approximately 200 W/cm^2, corresponding to an estimated intracavity laser power exceeding 500 mW that the SLM can safely withstand. The method proposed in this study provides an approach for designing the SLM projection phase to optimize the digital laser output intensity distribution such that it matches the target field intensity distribution, under the laser condition that the round-trip gain exceeds the round-trip loss. With regard to other structured-light properties—such as polarization, orbital angular momentum, and other related characteristics [29]—the extent to which SA-based optimization can be applied remains limited by the cavity design and therefore warrants further investigation. Finally, it is worth mentioning that the choice of cost function has a considerable influence on both the convergence speed and the final outcome of the SA method. Employing a varying cost function strategy [54]—by assigning different cost function settings to the high-amplitude regions of interest and the less critical low-amplitude regions—may provide a useful means of improving the optimization results.

4. Conclusions

This numerical study presents and validates a hybrid approach for designing SLM projection phases in digital lasers, combining the simulated annealing (SA) method with a pre-designed initial phase. By defining a cost function based on the correlation between the

target field and the current laser field, the proposed method optimizes the SLM projection phase to generate desired structured light patterns. Three geometric target fields—the quadrangular pyramid, triangular pyramid, and multi-ring field—were employed to verify the effectiveness of the SA-based phase design strategy. Comparisons with the conventional convolution method demonstrate that, although the convolution-designed phase achieves a high correlation with the target field, it produces smoothed features at the apex and edges. In contrast, the proposed SA method, initialized with the convolution-derived phase, yields laser fields that more accurately match the specified target, particularly enhancing edge sharpness and preserving fine structural details. Importantly, the proposed SA iteration framework is not limited to the L-shaped digital laser employed in this study. It can be extended to digital laser systems with higher numerical apertures, enabling the generation of more complex structured light fields. This potential extension warrants further investigation in future work.

Author Contributions: Conceptualization, S.-C.C.; Methodology, Y.-J.C. and S.-C.C.; Software, Y.-J.C.; Validation, Y.-J.C.; Formal analysis, Y.-J.C. and K.-C.C.; Investigation, Y.-J.C., K.-C.C. and T.-L.Y.; Data curation, Y.-J.C. and T.-L.Y.; Writing—original draft, Y.-J.C. and T.-L.Y.; Writing—review & editing, K.-C.C. and S.-C.C.; Supervision, S.-C.C.; Funding acquisition, S.-C.C. All authors have read and agreed to the published version of the manuscript.

Funding: This research was funded by National Science and Technology Council (NSTC 114-2112-M-006-018).

Data Availability Statement: Data underlying the results presented in this paper are not publicly available at this time but may be obtained from the authors upon reasonable request.

Conflicts of Interest: The authors declare no conflicts of interest.

Abbreviations

The following abbreviations are used in this study:

SA	Simulated Annealing
SLM	Spatial Light Modulator
DPSSL	Diode-Pumped Solid-State Laser
PM	Partially reflective Mirror

References

1. Leger, J.R.; Chen, D.; Wang, Z. Diffractive optical element for mode shaping of a Nd:YAG laser. *Opt. Lett.* **1994**, *19*, 108–110. [CrossRef]
2. Nakata, Y.; Osawa, K.; Miyanaga, N. Utilization of the high spatial-frequency component in adaptive beam shaping by using a virtual diagonal phase grating. *Sci. Rep.* **2019**, *9*, 4640. [CrossRef] [PubMed]
3. Zhu, L.; Wang, J. Arbitrary manipulation of spatial amplitude and phase using phase-only spatial light modulators. *Sci. Rep.* **2014**, *4*, 7441. [CrossRef] [PubMed]
4. Bélanger, P.A.; Lachance, R.L.; Paré, C. Super-Gaussian output from a CO_2 laser by using a graded-phase mirror resonator. *Opt. Lett.* **1992**, *17*, 739–741. [CrossRef] [PubMed]
5. Litvin, I.A.; Forbes, A. Intra–cavity flat–top beam generation. *Opt. Express* **2009**, *17*, 15891–15903. [CrossRef] [PubMed]
6. Yang, H.; Meng, J.; Chen, W. High efficiency and high-energy intra-cavity beam shaping laser. *Laser Phys.* **2015**, *25*, 095005. [CrossRef]
7. Caley, A.J.; Thomson, M.J.; Liu, J.S.; Waddie, A.J.; Taghizadeh, M.R. Diffractive optical elements for high gain lasers with arbitrary output beam profiles. *Opt. Express* **2007**, *15*, 10699–10704. [CrossRef]
8. Ngcobo, S.; Ait-Ameur, K.; Litvin, I.; Hasnaoui, A.; Forbes, A. Tuneable Gaussian to flat-top resonator by amplitude beam shaping. *Opt. Express* **2013**, *21*, 21113–21118. [CrossRef]
9. Ngcobo, S.; Litvin, I.; Burger, L.; Forbes, A. A digital laser for on-demand laser modes. *Nat. Commun.* **2013**, *4*, 2289. [CrossRef]
10. Tsai, K.-F.; Chu, S.-C. Generating laser output with arbitrary lateral shape by using multi-point beam superposition method in digital lasers. *Laser Phys.* **2018**, *28*, 075801. [CrossRef]

11. Huang, C.-Y.; Chang, K.-C.; Chu, S.-C. Experimental Investigation of Generating Laser Beams of on-Demand Lateral Field Distribution from Digital Lasers. *Materials* **2019**, *12*, 2226. [CrossRef]
12. Chu, S.-C.; Fu, Y.-X.; Chang, K.-C.; Huang, C.-Y. Generating a geometric structure light field from a digital laser by specifying a laser cavity phase boundary with a Gaussian-convoluted target field. *Opt. Express* **2021**, *29*, 35980–35992. [CrossRef]
13. Sandile, N.; Teboho, B.; Igor, A.L.; Darryl, N.; Kamel, A.-A.; Andrew, F. Selective excitation and detection of higher-order doughnut laser modes as an incoherent superposition of two petals modes in a digital laser resonator. *Proc. SPIE* **2015**, *2015*, 95810B. [CrossRef]
14. Gower, M.C. Industrial applications of laser micromachining. *Opt. Express* **2000**, *7*, 56–67. [CrossRef]
15. Visconti, P.; Turco, C.; Rinaldi, R.; Cingolani, R. Nanopatterning of organic and inorganic materials by holographic lithography and plasma etching. *Microelectron. Eng.* **2000**, *53*, 391–394. [CrossRef]
16. Yang, L.; El-Tamer, A.; Hinze, U.; Li, J.W.; Hu, Y.L.; Huang, W.H.; Chu, J.R.; Chichkoy, B.N. Parallel direct laser writing of micro-optical and photonic structures using spatial light modulator. *Opt. Lasers Eng.* **2015**, *70*, 26–32. [CrossRef]
17. MacDonald, M.P.; Paterson, L.; Volke-Sepulveda, K.; Arlt, J.; Sibbett, W.; Dholakia, K. Creation and Manipulation of Three-Dimensional Optically Trapped Structures. *Science* **2002**, *296*, 1101–1103. [CrossRef]
18. Daria, V.R.; Eriksen, R.L.; Glückstad, J. Dynamic optical manipulation of colloidal systems using a spatial light modulator. *J. Mod. Opt.* **2003**, *50*, 1601–1614. [CrossRef]
19. Eriksen, R.L.; Daria, V.R.; Rodrigo, P.J.; Glückstad, J. Computer-controlled orientation of multiple optically-trapped microscopic particles. *Microelectron. Eng.* **2003**, *67–68*, 872–878. [CrossRef]
20. Sanner, N.; Huot, N.; Audouard, E.; Larat, C.; Huignard, J.P. Direct ultrafast laser micro-structuring of materials using programmable beam shaping. *Opt. Lasers Eng.* **2007**, *45*, 737–741. [CrossRef]
21. Jenness, N.J.; Wulff, K.D.; Johannes, M.S.; Padgett, M.J.; Cole, D.G.; Clark, R.L. Three-dimensional parallel holographic micropatterning using a spatial light modulator. *Opt. Express* **2008**, *16*, 15942–15948. [CrossRef]
22. Obata, K.; Koch, J.; Hinze, U.; Chichkov, B.N. Multi-focus two-photon polymerization technique based on individually controlled phase modulation. *Opt. Express* **2010**, *18*, 17193–17200. [CrossRef]
23. Gittard, S.D.; Nguyen, A.; Obata, K.; Koroleva, A.; Narayan, R.J.; Chichkov, B.N. Fabrication of microscale medical devices by two-photon polymerization with multiple foci via a spatial light modulator. *Biomed. Opt. Express* **2011**, *2*, 3167–3178. [CrossRef] [PubMed]
24. Zhang, S.-J.; Li, Y.; Liu, Z.-P.; Ren, J.-L.; Xiao, Y.-F.; Yang, H.; Gong, Q. Two-photon polymerization of a three dimensional structure using beams with orbital angular momentum. *Appl. Phys. Lett.* **2014**, *105*, 061101. [CrossRef]
25. Ni, J.; Wang, C.; Zhang, C.; Hu, Y.; Yang, L.; Lao, Z.; Xu, B.; Li, J.; Wu, D.; Chu, J. Three-dimensional chiral microstructures fabricated by structured optical vortices in isotropic material. *Light Sci. Appl.* **2017**, *6*, e17011. [CrossRef]
26. Wang, J.; Yang, J.-Y.; Fazal, I.M.; Ahmed, N.; Yan, Y.; Huang, H.; Ren, Y.; Yue, Y.; Dolinar, S.; Tur, M.; et al. Terabit free-space data transmission employing orbital angular momentum multiplexing. *Nat. Photonics* **2012**, *6*, 488–496. [CrossRef]
27. Willner, A.E.; Huang, H.; Yan, Y.; Ren, Y.; Ahmed, N.; Xie, G.; Bao, C.; Li, L.; Cao, Y.; Zhao, Z.; et al. Optical communications using orbital angular momentum beams. *Adv. Opt. Photonics* **2015**, *7*, 66–106. [CrossRef]
28. Wang, J. Advances in communications using optical vortices. *Photonics Res.* **2016**, *4*, B14–B28. [CrossRef]
29. Forbes, A. Structured Light from Lasers. *Laser Photonics Rev.* **2019**, *13*, 1900140. [CrossRef]
30. Ren, Z.-C.; Fan, L.; Cheng, Z.-M.; Liu, Z.-F.; Lou, Y.-C.; Huang, S.-Y.; Chen, C.; Li, Y.; Tu, C.; Ding, J.; et al. On-demand orbital angular momentum comb from a digital laser. *Optica* **2024**, *11*, 951–961. [CrossRef]
31. Forbes, A.; Mkhumbuza, L.; Feng, L. Orbital angular momentum lasers. *Nat. Rev. Phys.* **2024**, *6*, 352–364. [CrossRef]
32. Fan, W.-Q.; Jia, S.-Q.; Fan, L.; Ding, J.; Ren, Z.-C.; Wang, X.-L.; Wang, H.-T. Cavity-enhanced nonlinear frequency conversion and manipulation of vector fields. *APL Photonics* **2025**, *10*, 036113. [CrossRef]
33. Chen, X.; Liu, S.; Lin, Z.; Chen, Z.; Pu, J. Dual-cavity digital laser for intra-cavity mode shaping and polarization control. *Opt. Express* **2018**, *26*, 18182–18189. [CrossRef] [PubMed]
34. Teboho, B.; Sandile, N. Intracavity second harmonic generation for higher-order laser modes. *Proc. SPIE* **2019**, *2019*, 109041P. [CrossRef]
35. Matsuura, T.; Takai, T.; Iwata, F. Local electrophoresis deposition assisted by laser trapping coupled with a spatial light modulator for three-dimensional microfabrication. *Jpn. J. Appl. Phys.* **2017**, *56*, 105502. [CrossRef]
36. Tradonsky, C.; Mahler, S.; Cai, G.; Pal, V.; Chriki, R.; Friesem, A.A.; Davidson, N. High-resolution digital spatial control of a highly multimode laser. *Optica* **2021**, *8*, 880–884. [CrossRef]
37. Kirkpatrick, S.; Gelatt, C.D.; Vecchi, M.P. Optimization by Simulated Annealing. *Science* **1983**, *220*, 671–680. [CrossRef]
38. Rere, L.M.R.; Fanany, M.I.; Arymurthy, A.M. Simulated Annealing Algorithm for Deep Learning. *Procedia Comput. Sci.* **2015**, *72*, 137–144. [CrossRef]
39. Porth, L.; Boyd, M.; Pai, J. Reducing Risk Through Pooling and Selective Reinsurance Using Simulated Annealing: An Example from Crop Insurance. *Geneva Risk Insur. Rev.* **2016**, *41*, 163–191. [CrossRef]

40. Ibn Majdoub Hassani, Z.; El Barkany, A.; Jabri, A.; El Abbassi, I.; Darcherif, A.M. A Comparative Analysis of Metaheuristic Approaches (Genetic Algorithm/Hybridization of Genetic Algorithms and Simulated Annealing) for Planning and Scheduling Problem with Energy Aspect. *SAE Int. J. Mater. Manuf.* **2021**, *14*, 363–374. [CrossRef]
41. El-Agmy, R.; Bulte, H.; Greenaway, A.H.; Reid, D.T. Adaptive beam profile control using a simulated annealing algorithm. *Opt. Express* **2005**, *13*, 6085–6091. [CrossRef]
42. Hao, B.; Leger, J. Polarization beam shaping. *Appl. Opt.* **2007**, *46*, 8211–8217. [CrossRef]
43. Yu, Z.; Ma, H.; Du, S. Simulated annealing algorithm applied in adaptive near field beam shaping. *Proc. SPIE* **2010**, *2010*, 78480Q. [CrossRef]
44. Hu, C.; Xiao, Y.; He, Y.; Liu, Y.; Song, Y.; Tang, X. Optimization of brightness in a Nd:YAG laser by maximizing the single-mode power factor with an intra-cavity spatial light modulator. *Appl. Opt.* **2022**, *61*, 1482–1491. [CrossRef] [PubMed]
45. Endo, M.; Kawakami, M.; Nanri, K.; Takeda, S.; Fujioka, T. Two-dimensional simulation of an unstable resonator with a stable core. *Appl. Opt.* **1999**, *38*, 3298–3307. [CrossRef] [PubMed]
46. Endo, M.; Yamaguchi, S.; Uchiyama, T.; Fujioka, T. Numerical simulation of the w-axicon type optical resonator for coaxial slab CO_2 lasers. *J. Phys. D Appl. Phys.* **2001**, *34*, 68. [CrossRef]
47. Endo, M. Numerical simulation of an optical resonator for generation of a doughnut-like laser beam. *Opt. Express* **2004**, *12*, 1959–1965. [CrossRef]
48. Chu, S.-C.; Otsuka, K. Numerical study for selective excitation of Ince-Gaussian modes in end-pumped solid-state lasers. *Opt. Express* **2007**, *15*, 16506–16519. [CrossRef]
49. Ohtomo, T.; Chu, S.-C.; Otsuka, K. Generation of vortex beams from lasers with controlled Hermite- and Ince-Gaussian modes. *Opt. Express* **2008**, *16*, 5082–5094. [CrossRef]
50. Chu, S.-C.; Tsai, K.-F. Numerical study for selective excitation of Mathieu-Gauss modes in end-pumped solid-state laser systems. *Opt. Express* **2011**, *19*, 3236–3250. [CrossRef] [PubMed]
51. Metropolis, N.; Rosenbluth, A.W.; Rosenbluth, M.N.; Teller, A.H.; Teller, E. Equation of State Calculations by Fast Computing Machines. *J. Chem. Phys.* **1953**, *21*, 1087–1092. [CrossRef]
52. Fisher, R.A. *Statistical Methods for Research Workers*, 13th ed.; Hafner: New York, NY, USA, 1958.
53. Kendall, M.G. *The Advanced Theory of Statistics*, 4th ed.; Macmillan: London, UK, 1979.
54. Khonina, S.N.; Kotlyar, V.V.; Skidanov, R.V.; Soifer, V.A. Levelling the focal spot intensity of the focused gaussian beam. *J. Mod. Opt.* **2000**, *47*, 883–904. [CrossRef]